scientific reports

Check for updates

OPEN

2-Methoxyestradiol attenuates lung injury induced by chronic intermittent hypoxia via inhibiting the HIF1-α/SLC7A11 pathway

Jia Chen[1,2,3], Hansheng Xie[1,2,3], Wenqian Chen[1,2,3], Ting Lin[1,2,3], Shiyuan Huang[1,2,3], Yaqi Liu[1,2,3], Jiefeng Huang[1,2,3] & Ningfang Lian[1,2,3]✉

Ferroptosis is a novel type of programmed cell death associated with lung injury induced by chronic intermittent hypoxia (CIH). 2-Methoxyestradiol (2-ME2), as an inhibitor of Hypoxia-inducible factor 1 alpha (HIF-1α), affects HIF-1α-related biological processes. This study aimed to explore the role and mechanism of 2-ME2 on CIH-induced lung injury. CIH-associated lung injury was verified in SD rats. 2-ME2 was administered intraperitoneally at a dosage of 20 mg/kg to verify its treatment efficacy. CIH treated Human bronchoalveolar epithelial cells (BEAS-2B) were used to explore the mechanism of 2-ME2. HIF-1α knockdown cell lines and SLC7A11-overexpressing cell lines were established to explore the role of HIF-1α/SLC7A11 pathway in CIH-induced ferroptosis. The ChIP-qPCR was employed to determine the presence of binding sites between HIF-1α and the SLC7A11 promoter region. In vivo experiments demonstrated that, in comparison with the control group, there was an increase in lung injury scores and collagen ratio in the lung tissue of rats belonging to the CIH group, along with an upregulation of HIF-1α expression and alterations in the expression of ferroptosis-related genes (all $p < 0.05$). 2-ME2 mitigated the lung injury and ferroptosis induced by CIH in vivo. In vitro experiments revealed that, compared to BEAS-2B cells under normoxic conditions, HIF-1α expression increased significantly in BEAS-2B cells exposed to CIH. This was accompanied by alterations in the expression of ferroptosis-related genes (all $p < 0.05$) and an increase in both reactive oxygen species (ROS) and Fe^{2+} levels (both $p < 0.05$). HIF-1α knockdown, or SLC7A11 overexpression, reversed CIH-induced BEAS-2B cell ferroptosis. ChIP-qPCR confirmed the direct interaction between HIF-1α and SLC7A11 promoter region. The HIF-1α inhibitor, 2-ME2, effectively reverses CIH-induced lung tissue ferroptosis. The potential mechanism of 2-ME2 in inhibiting ferroptosis may involve suppressing the HIF-1α/SLC7A11 pathway.

Keywords Obstructive sleep apnea, Chronic intermittent hypoxia, HIF-1α, SLC7A11, Ferroptosis, Lung injury

Abbreviations

OSA	obstructive sleep apnea
CIH	chronic intermittent hypoxia
SD	Sprague-Dawley
BEAS-2B	Human bronchial epithelial cell line
HIF-1α	hypoxia-inducible factor-1α
SLC7A11	cystine/glutamate antiporter solute carrier family 7 member 11
GPX4	glutathione peroxidase 4
CCK-8	cell counting kit-8
ROS	reactive oxygen species
siRNA	small interfering RNA

[1]Department of respiratory and critical care medicine, Respiratory Disease Research Institute, the First Affiliated Hospital, Fujian Medical University, No 20, Chazhong Road, Taijiang District, Fuzhou 350005, Fujian, People's Republic of China. [2]Fujian Provincial Sleep-disordered Breathing Clinic Center, Fuzhou, China. [3]Department of respiratory and critical care medicine, Binhai Campus of the First Affiliated Hospital, National Regional Medical Center, Fujian Medical University, Fuzhou 350212, China. ✉email: 1533532863@qq.com

2-ME2	2-methoxyestradiol
HE	Hematoxylin-eosin
COPD	chronic obstructive pulmonary disease
CPAP	Continuous positive airway pressure
CRP	C-reactive protein
TNF-α	tumor necrosis factor-alpha
FcO2	fractional oxygen concentration
HEPA	High efficiency particulate air Filter
RPMI	Roswell park memorial institute
RIPA	Radio Immunoprecipitation Assay
SDS-PAGE	sodium dodecyl sulfate-polyacrylamide gel electrophoresis
TBST	Tris Buffer Solution Tween
PBS	phosphate-buffered saline
CCK-8	Cell counting kit-8
DCFH-DA	2',7'-Dichlorodihydrofluorescein diacetate
HCA	hydroxycitric acid
GSH	glutathione
HSCs	hepatic stellate cells
METTL14	methyltransferase- like 14
YTHDF2	YTH domain family 2
HCC	hepatocellular carcinoma

Obstructive sleep apnea (OSA) is a prevalent chronic respiratory disease which is characterized by recurrent episodes of upper airway collapse during sleep and a characteristic pathophysiological feature of chronic intermittent hypoxia (CIH)[1,2]. Existing evidence showed that OSA induced multi-system complications[3–6]. The previous clinical studies confirmed that OSA was associated with lung injury. OSA exacerbated the inflammation levels in patients diagnosed with chronic obstructive pulmonary disease (COPD), including the levels of interleukin-6, C-reactive protein (CRP), and tumor necrosis factor-alpha (TNF-α)[7–10]. Furthermore, multiple clinical types of research suggested that OSA accelerated the decline in lung function in patients with chronic respiratory diseases, including asthma, COPD, pulmonary arterial hypertension, and interstitial lung disease[3,11–15]. Untreated OSA increased the rate of acute exacerbations and rehospitalizations in COPD patients[16–18]. However, the mechanism of lung injury associated with OSA remains unclear.

Ferroptosis is a distinct form of programmed cell death[19]. Recent research has reported that CIH leads to an increase in reactive oxygen species (ROS) and causes oxidative stress overload, resulting in a losing imbalance between oxidation and antioxidation, leading to ferroptosis, which is involved in CIH-related lung injuries[20]. However, previous studies have merely observed ferroptosis as a phenotype that occurs after CIH treatment, without delving into the underlying mechanisms responsible for CIH-related ferroptosis.

Hypoxia-inducible factor 1 alpha (HIF-1α) is a vital transcription factor[21,22]. The elevation of HIF-1α was associated with various complications related to OSA, such as insulin resistance, hypertension, and cognitive dysfunction[23]. When CIH occurred, the expression of HIF-1α increased, leading to the activation of HIF-1α-dependent pro-oxidant enzyme genes and subsequent elevation of ROS[24,25]. Furthermore, studies have shown that the activation of HIF-1α caused ferroptosis[26]. Therefore, we speculate that HIF-1α may play a certain role in CIH-related lung injury.

2-Methoxyestradiol (2-ME2) is an effective inhibitor of HIF-1α, exhibiting anti-angiogenic, anti-proliferative, and pro-apoptotic properties[27]. Recently, research has proved that 2-ME2 relieved oxidative injury and mitigated ischemia/reperfusion (IR)-induced lung inflammation and lung injury in an IR rat model[28]. 2-ME2 downregulation of the expression of HIF-1α reduced the rate of collagen deposition and mitigated lung injury induced by radiation[29]. Given the biological activity of 2-ME2, it may become a potential candidate drug for HIF-1α activating. Nevertheless, the effect of 2-ME2 on the lung tissue ferroptosis associated with CIH remains elusive.

This study aimed to explore the role of HIF-1α activation in CIH-induced lung injury and preliminarily investigate the therapeutic efficacy of HIF-1α inhibitor, 2-ME2.

Methods

Construction of animal models

The Sprague-Dawley (SD) rats, which were aged 8 weeks, were obtained from Fujian Medical University and kept in a stabilized environment with 12 h light and 12 h dark cycles and accessed water and food freely. The computer random number method was used to divide the SD rats into the control group, CIH group, CIH + Vehicle group, and CIH + 2-ME2 group. The control rats were exposed to normal air. The CIH group rats were placed in an intermittent hypoxic chamber for 8 h each day, lasting for 12 weeks, to simulate moderate OSA. The brief process is as follows: An intermittent low-oxygen tank controlled by a computer created a CIH environment. Nitrogen was pumped into the tank for 120 s to decrease the fractional oxygen concentration (FcO2) to 6%, which was then stabilized for an additional 30 s. Subsequently, oxygen was pumped into the tank to reoxygenation it to 21% for 10 s and maintained for 20s[20]. The CIH + 2-ME2 group underwent daily intraperitoneal injections of 20 mg/kg 2-ME2 for the final 4 weeks of the modeling process. The CIH + 2-ME2 group received an intraperitoneal injection of 20 mg/kg of 2-ME2 (2-ME2 was dissolution in a solution containing 8% DMSO, 40% PEG300, 2% Tween 80, and 50% normal saline) for 4 weeks after 8 weeks of CIH. CIH + Vehicle group received an intraperitoneal injection consisting of a solution containing 8% DMSO, 40% PEG300, 2% Tween 80, and 50% normal saline. All rats in this study were treated following humane guidelines and followed the ARRIVE

guidelines. After a 12-week modeling process, euthanasia was performed to collect lung tissue. Euthanasia was conducted by intraperitoneal injection of pentobarbital sodium at a dose of 50 mg/kg. This study was approved by the Ethics Committee of the Fujian Medical University Laboratory Animal Center. The approval number is IACUCFJMU2022-0031.

Hematoxylin-eosin (HE) staining and Masson staining

The lung tissue was fixed with 4% paraformaldehyde and then underwent dehydrated, transparency, and embedded in paraffin wax. The lung wax blocks were sliced into sections with a thickness of approximately 4 μm. After staining with hematoxylin and eosin or Masson's trichrome, the sections were examined via a light microscope (Olympus BX50, Tokyo, Japan). The lung injury score and collagen deposition rate were calculated according to the method described in the literature[30,31]. Two pathologists who independently analyzed each section obtained the lung injury score. Three high-power fields (200×) were selected for scoring for each section. The total score was the average from four parts, which included interstitial edema, inflammatory cell infiltration, alveolar hemorrhage, and alveolar edema; each scored on a scale of 0–4: 0, no injury; 1, 25% injury; 2, 50% injury; 3, 75% injury; and 4, 100% injury[32,33].

Construction of cell models

Human bronchoalveolar epithelial cells (BEAS-2B) (Beyotime, China) were cultured in a CO_2 incubator (37 °C, 5% CO_2). The culture medium was Roswell Park Memorial Institute (RPMI) 1640 (Hyclone Laboratories, Utah, USA) supplemented with 10% fetal bovine serum) (Gibco, CA, USA) and 1% penicillin-streptomycin (Beyotime, China). A hypoxia incubator (Thermo Fisher Scientific, Boston, USA) with a High-efficiency particulate air Filter (HEPA) was utilized to create a cyclic intermittent hypoxia condition. The CIH condition, which consisted of 1 h of hypoxia followed by 0.5 h of normal oxygen, lasted 36 h. Each cell experiment consisted of three independently repeated trials.

Establishment of HIF-1α knockdown cell line

We constructed a HIF-1α-knockdown cell line. When the cell growth density was approximately 40% in a six-well plate, we combined 8 μL of Lipofectamine RNAi MAX transfection reagent (Genepharma, Shanghai) with 10μL of HIF-1α-siRNA/ Control-siRNA (50nM), following the guidelines provided by the manufacturer. After 6 h of transfection, the cells were transferred into a complete culture medium of RPMI 1640 supplemented with 10% fetal bovine serum and cultured for an additional 24 h. Then, we used the HIF-1α-knockdown cell line to do the following experiments. The target sequence of siRNA is presented in Table 1.

Establishment of SLC7A11-overexpressing cell line

The SLC7A11 overexpressing plasmid vector and the control overexpressing vector were compounded by GenePharma (Shanghai, China). The lentivirus was packaged in 293T cells and collected from the culture medium supernatant. BEAS-2B cells were transfected with lentivirus for 24 h and were screened with puromycin after 72 h to establish stable cell lines.

qRT-PCR

Total RNA was isolated using an RNA extract kit (Vazyme, China), and then the transcription was reversed to cDNA. qRT-PCR was used to detect the mRNA expression levels. All steps were following the guidelines provided by the manufacturer. The relative gene expression was computed using the $2^{-\Delta\Delta Ct}$ Method. The sequences of mRNA primers are shown in Table 2.

Chromatin Immunoprecipitation assay (ChIP)

Based on the information from the Jasper database (http://jaspar.genereg.net/), possible binding sites of the transcription factor HIF-1a with the SLC7A11 promoter have been predicted. To verify the prediction results, CHIP-PCR was carried out. ChIP was performed on BEAS-2B cells after 24 h of CIH treatment, following the manufacturer's guidelines (Beyotime, China). After 10 min of cross-linking with 1% formaldehyde at 37 ° C, we added 10× glycine solution for 5 min at room temperature, and added 5–10 ml pre-cooled 1mM PMSF and washed the cells three times. The cells were then resuspended in an SDS lysis buffer, and the DNA was ultrasonically fragmented into 200 bp fragments. The pre-cleared chromatin was incubated overnight with HIF-1α (CST) or IgG antibodies. Protein A agarose beads were added, and the mixture was incubated at 4℃ for 1 h. After decrosslinking, the DNA was collected, and then purified according to kit instructions (Beyotime, China). qRT-PCR was used to detect DNA expression levels. The primer sequences employed for ChIP-qPCR are in Table 3. The calculation for % Input was as follows: % Input = 2 (-ΔCt [normalized ChIP]) x 100%.

Genes	Primer sequence
Human-HIF-1α-siRNA	F: CCAGCAGACUCAAAUACAATT
	R: UUGUAUUUGAGUCUGCUGGTT
Human-Control-siRNA	F: UUCUCCGAACGUGUCACGUTT
	R: ACGUGACACGUUCGGAGAATT

Table 1. The target sequence of SiRNA of HIF-1α.

Genes	Primer sequence
Rat-HIF-1α	F: TCAGTTGTCACCATTAGAGA
	R: TCTATATTGTCCTTCGTCACT
Rat-SLC7A11	F: CCTGTTGTGTCCACCATCTC
	R: GATGAAGATTCCTGCTCCAATGA
Rat-GPX4	F: CCGCTGTGGAAGTGGATGAAGATC
	R: CTTGTCGATGAGGAACTGTGGAG
Rat-β-ACTIN	F: TGGCACCCAGCACAATGAA
	R: CTAAGTCATAGTCCGCCTAGAAGCA
Hsa-HIF-1α	F: AGTGTACCCTAACTAGCCGA
	R: CACAAATCAGCACCAAGC
Hsa-SLC7A11	F: CCTGTTGTGTCCACCATCTC
	R: GATGAAGATTCCTGCTCCAATGA
Hsa-GPX4	F: CCGCTGTGGAAGTGGATGAAGATC
	R: CTTGTCGATGAGGAACTGTGGAG
Hsa-β-ACTIN	F: TGGCACCCAGCACAATGAA
	R: CTAAGTCATAGTCCGCCTAGAAGCA

Table 2. PCR primer sequence.

Gene SLC7A11	Location (TSS)	Primer sequence
ChIP 1	− 658~-557	F: TGTATTAGTCACACTCGGATGGT
		R: CACACAACTATAAGCCTTCCTCA
ChIP 2	46 ~ 165	F: GGAACGAGGAGGTGGAGAAT
		R: GCGCTATAGTGTTCACAGGTG
ChIP 3	467 ~ 662	F: TCATCTCTCCTAAGGGCGTG
		R: GCCTTTGCCATCCATTCACT

Table 3. Chip-qPCR primer sequence.

Western blot

After modeling, cells or lung tissue were pyrolyzed by Radio Immunoprecipitation Assay (RIPA) buffer with 1% PMSF. The protein samples were isolated by SDS-PAGE and then transferred to PVDF membranes. Following a 1 h blocking step in 5% skim milk, the membranes were subsequently incubated overnight at 4 °C with specific antibodies against HIF-1α (1:1000, CST), SLC7A11 (1:500, Abcam), and GPX4 (1:1000, Abcam). The membranes were washed by TBST three times to remove unbound antibodies. Subsequently, they were soaked in a secondary antibody (1:100000, HUABIO) for 1 h. After three additional washes with TBST, the bands were visualized using the chemiluminescence detection system. The analysis of protein band gray values was performed using Image J. The original blot images are shown in Figure S2.

Cell counting Kit-8 (CCK-8) assay

10^4 cells were planted in a 96-well plate. After modeling, each well was incubated with a 10% CCK-8 solution (Beyotime, China) at 37 °C for 2 h. A microplate reader was used to measure the absorbance at 450 nm.

Apoptosis assay

The cell culture supernatant was collected. The cells were digested using EDTA-free trypsin and combined with the supernatant to collect them all. The cells were washed twice with pre-chilled PBS and then gently resuspended in 100 μL of pre-chilled 1× Binding Buffer. Subsequently, 5 μL of Annexin V-FITC and 5 μL of PI pre-mixture were added, and the cells were incubated the cells at room temperature for 8–10 min. Then, 400 μL of pre-cooled 1× Binding Buffer was added and gently mixed. Finally, within an hour, the cells were analyzed using a C6 flow cytometer (Becton Dickinson, USA).

ROS level

To assess intracellular ROS levels in BEAS-2B cells, the fluorescence probe 2',7'-Dichlorodihydrofluorescein diacetate (DCFH-DA) was employed. After collecting the cells, they were incubated with 10 μM DCFH-DA (Beyotime, China) for 20 min in a 37 °C incubator, with gentle mixing every 3–5 min during the incubation period. Subsequently, the cells were washed three times with non-serum 1640 and analyzed using a C6 cytometry system (Becton Dickinson, USA).

Fe^{2+} level

FerroOrange (F-374, Dojindo, China) was used to detect the presence of Fe^{2+} in the BEAS-2B cells. After collection, the cells were washed three times with non-serum 1640, followed by a 30-minute incubation with 1 μM FerroOrange. Subsequently, the cells were analyzed using a C6 cytometry system (Becton Dickinson, USA).

Statistical analysis

Statistical analysis was conducted using GraphPad 7.0 software from GraphPad Software Inc. (USA). To compare the means of multiple samples, Analysis of Variance (ANOVA) was employed. If the results of the ANOVA indicated a significant difference, then a t-test was conducted to compare the means between two specific groups. Mean ± SD values were reported. A P-value < 0.05 indicates a significant difference.

Results

HIF-1α was upregulated and ferroptosis occurred in CIH-treated rats

A rat animal model was constructed to observe CIH-induced lung injury through in vivo experiments. HE staining and Masson staining were performed to evaluate the histopathological alteration after CIH treatment. HE staining revealed the presence of interstitial hyperemia, edema, and inflammatory cell infiltration in the CIH group, which led to higher lung injury scores (Fig. 1A, B). Masson staining revealed a significant increase in the collagen ratio in the CIH group, compared with that in the control group ($p < 0.05$) (Fig. 1C, D). Interestingly, compared with the control group, the expression levels of HIF-1α were significantly upregulated, and the expression levels of ferroptosis-related genes, GPX4 and SLC7A11, were significantly downregulated in the lung tissue of rats (Fig. 1E, F).

HIF-1α inhibitor, 2-ME2 alleviated lung tissue injury and ferroptosis induced by CIH

2-ME2 is an HIF-1α inhibitor. The role of 2-ME2 in CIH-induced lung injury was observed through in vivo experiments. After the 2-ME2 treatment, a notable reduction in lung injury scores was observed through HE staining ($p < 0.05$) (Fig. 2A, B). Additionally, Masson staining revealed that 2-ME2 treatment mitigated the collagen ratio in lung tissue (both $p < 0.05$) (Fig. 2C, D). Meanwhile, 2-ME2 treatment effectively reversed the altered mRNA and protein expression levels of SLC7A11 and GPX4 in the CIH group (both $p < 0.05$) (Fig. 2E, F).

HIF-1α was upregulated and ferroptosis occurred in CIH-treated BEAS-2B

BEAS-2B cells were used to observe the effects of CIH on lung injury in vitro. The CCK-8 assay revealed a decrease in cell viability in CIH-treated BEAS-2B (Fig. 3B). Flow cytometry analysis demonstrated increased levels of apoptosis rates, ROS, and Fe^{2+} in CIH-treated BEAS-2B (Fig. 3A, C, D). Compared with BEAS-2B in normoxic conditions, the expression level of HIF-1α was upregulated, while the expression levels of the ferroptosis-related genes, GPX4 and SLC7A11, were downregulated in CIH-treated BEAS-2B (Fig. 3E, F).

HIF-1α/ SLC7A11 signal pathway played a role in CIH-induced BEAS-2B ferroptosis

To clarify the role of HIF-1α in CIH-related lung injury, we constructed a HIF-1α-knockdown cell line using the siRNA method. The knockdown efficiency of HIF-1α was verified through qRT-PCR and Western Blot analysis (Fig. 4A, B). After HIF-1α knockdown, the detrimental effects of CIH on BEAS-2B, including decreased cell viability, increased apoptosis rate, elevated ROS levels, and increased Fe^{2+} levels, were all reversed (Fig. 4C, D, E, F). Additionally, HIF-1α knockdown counteracted the alterations in the expression levels of SLC7A11 and GPX4 in CIH-treated BEAS-2B cells (Fig. 4G, H).

To clarify the role of SLC7A11 in CIH-related lung injury, SLC7A11 overexpressed BEAS-2B cells were constructed using lentivirus transfection. The efficiency of SLC7A11 overexpression was confirmed through qRT-PCR and Western Blot analysis (Fig. 5A, B). After SLC7A11 overexpression, the detrimental effects of CIH on BEAS-2B, including decreased cell viability, increased apoptosis rate, elevated ROS levels, and increased Fe^{2+} levels, were all effectively reversed (Fig. 5C, D, E, F). Furthermore, SLC7A11 overexpression reversed the altered expression levels of GPX4 in CIH-treated BEAS-2B cells, while HIF-1α mRNA and protein levels remained unchanged (Fig. 5G, H).

The prediction of HIF-1α binding sites within the promoter region of SLC7A11 is presented in Table 4. We further conducted a ChIP-qPCR analysis to confirm the interaction between HIF-1α and the promoter region of SLC7A11 after 24 h CIH treatment. The results revealed significant enrichment of HIF-1α at the following positions within the promoter region of the SLC7A11 gene: -658 to -557 bp, 46 to 165 bp, and 467 to 662 bp, respectively (Fig. 5I).

Discussion

In our study, we found CIH-induced lung injury and HIF-1α upregulated both in vivo and in vitro. HIF-1α inhibitor, 2-ME2 treatment reversed CIH-induced lung injury in vivo. The knockdown of HIF-1α ameliorated CIH-related lung injury and ferroptosis in vitro via SLC7A11.

The prevalence of respiratory diseases such as chronic cough, COPD, asthma, pulmonary hypertension, and pulmonary fibrosis is elevated among patients with OSA[3,11–15]. In our study, compared to the control group, the pathology results showed an increased lung injury score and an increased rate of collagen deposition in the CIH group. Therefore, CIH-related lung injury was confirmed. However, few studies have focused on ferroptosis in CIH-induced lung injury.

Ferroptosis is a form of programmed cell death dependent on iron, first identified in 2012[19]. It involves the accumulation of iron within cells, extensive generation of ROS, and lipid peroxidation[34]. SLC7A11 is a critical component of the antioxidant system as an iron-regulated apoptotic modulator that maintains redox

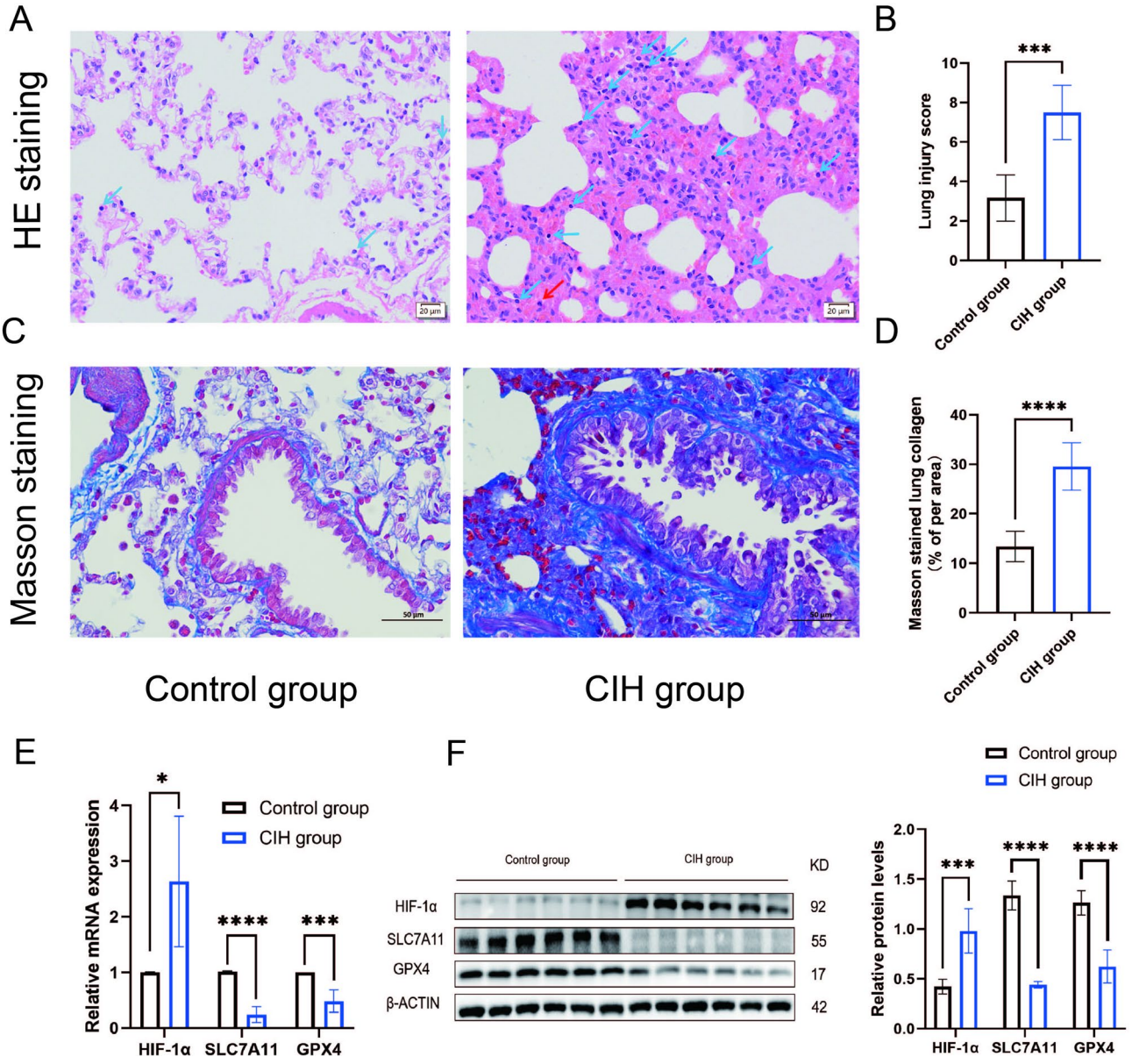

Fig. 1. CIH-induced lung tissue injury and ferroptosis-related gene expression changes ($n = 6$). (**A**) HE staining. Blue arrows indicate lymphocytes, red arrows indicate neutrophils; (**B**), Lung injury score; (**C**), Masson staining; (**D**), The proportion of collagen areas in lung tissue. (**E**), CIH upregulated HIF-1α mRNA while downregulating SLC7A11 and GPX4 mRNA compared with the control group; (**F**), CIH upregulated HIF-1α protein and reduced SLC7A11 and GPX4 protein levels compared with the control group. Data are shown as the mean ± SD. * $p < 0.05$; *** $p < 0.001$; **** $p < 0.0001$.

homeostasis[35]. GPX4 is an intracellular selenium-containing antioxidant enzyme that is a crucial regulator of ferroptosis[36]. In our study, we observed the expression levels of SLC7A11 and GPX4 downregulation in the CIH group both in vivo and in vitro. Furthermore, the elevated levels of ROS and iron ions in vitro suggested the occurrence of ferroptosis in alveolar epithelial cells induced by CIH. However, the underlying mechanism of CIH-induced ferroptosis is not clear.

2-ME2 is an effective inhibitor of HIF-1α, exerting pharmacological effects that include anti-angiogenic, anti-proliferative, and pro-apoptotic properties[27], and it has been widely used in clinical trials[37]. In our study, the rats were administered 2-ME2 intraperitoneally at a 20 mg/kg dose for 4 weeks during the experiment. 2-ME2 treatment mitigated lung injury induced by CIH, reduced HIF-1α expression levels, and reversed the expression levels of ferroptosis-related proteins. The results indicate that 2-ME2 has potential therapeutic effects on CIH-related lung injury, and this therapeutic effect may be associated with 2-ME2's inhibitory action on HIF-1α.

HIF-1α, a master transcriptional regulator of hypoxia[21,22]. Several clinical studies found increased levels of HIF-1α protein in patients with OSA[38–40]. SLC7A11 is a critical component of the antioxidant system as a ferroptosis modulator that maintains redox homeostasis[35]. The role of the HIF-1α/SLC7A11 signaling pathway

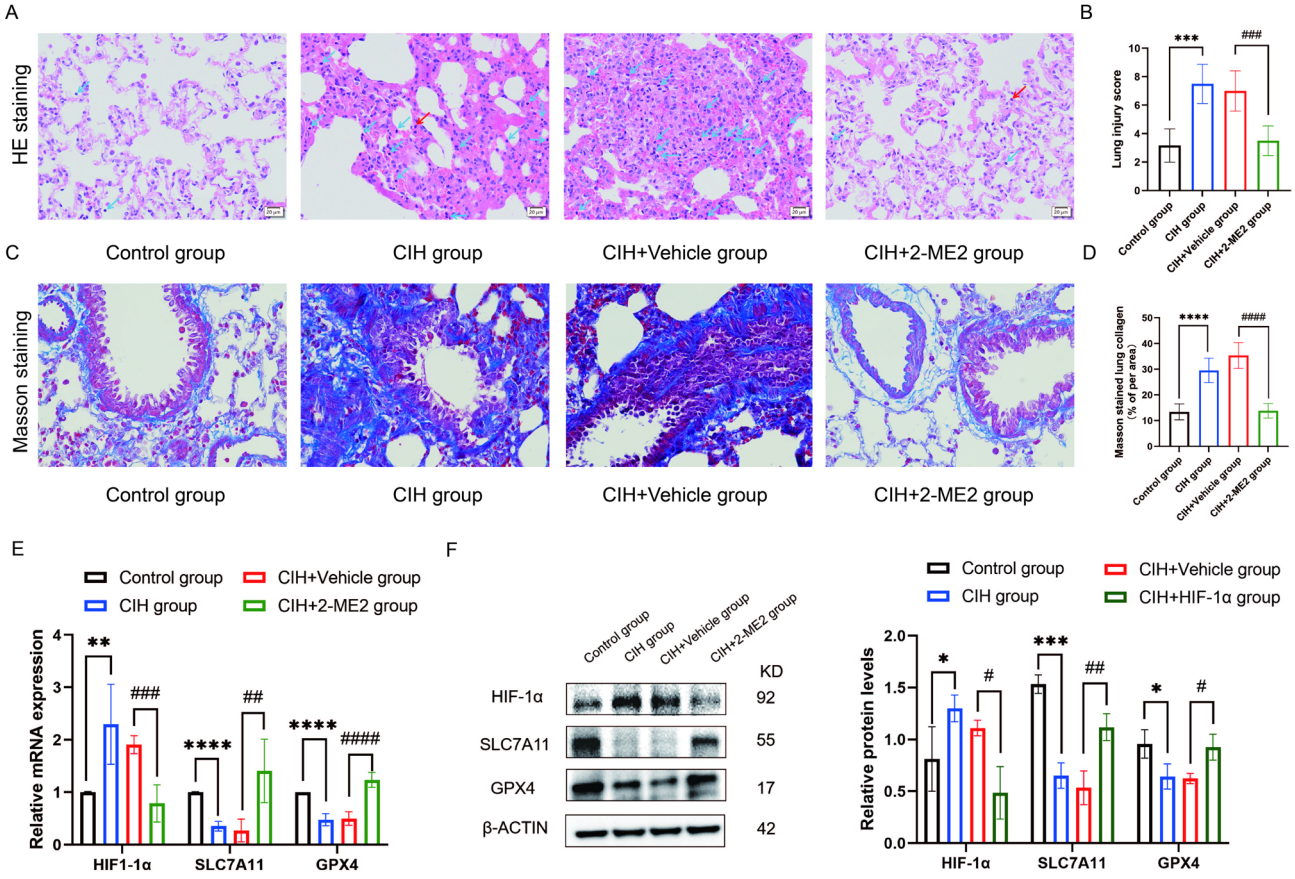

Fig. 2. 2-ME2 reversed CIH-induced lung tissue injury and ferroptosis in SD rats ($n = 6$). (**A**,**B**), HE staining showed that the treatment of 2-ME2 reversed the lung injury induced by CIH compared to the CIH + Vehicle group. Blue arrows indicate lymphocytes, red arrows indicate neutrophils; (**C**,**D**) Masson staining showed that the treatment of 2-ME2 reversed the ratio of collagen deposition induced by CIH compared to the CIH + Vehicle group. (**E**) 2-ME2 treatment decreased HIF-1α mRNA levels, reversed SLC7A11 and GPX4 mRNA levels. (**F**), 2-ME2 treatment decreased HIF-1α protein levels, reversed SLC7A11 and GPX4 protein levels. Data are shown as the mean ± SD. CIH group compared with control group: * $p < 0.05$; ** $p < 0.01$; *** $p < 0.001$; **** $p < 0.0001$; CIH + 2-ME2 group compared with CIH + Vehicle group: # $p < 0.05$; ## $p < 0.01$; ### $p < 0.001$; #### $p < 0.0001$.

on ferroptosis received increasing attention. Yuan et al. demonstrated that the activation of the HIF-1α/SLC7A11 signaling pathway triggers ferroptosis in hepatic stellate cells (HSCs), ameliorating liver injury and fibrosis[41]. Fan et al. discovered that hypoxia regulates ferroptosis in HCC cells and identified the HIF-1α/ methyltransferase-like 14 (METTL14)/ YTH domain family 2 (YTHDF2)/SLC7A11 axis as a potential therapeutic target for hepatocellular carcinoma (HCC) treatment[42]. Chen et al. observed an upregulation of HIF-1 expression and a concurrent downregulation of SLC7A11 expression in rhabdomyolysis (RM)-induced acute kidney injury (AKI) rats[43]. The unstable regulatory relationships of HIF-1α and SLC7A11 may be related to differences in cell types and disease types. In our study, HIF-1α silencing and SLC7A11 overexpression both alleviated CIH-related lung injury. HIF-1α silencing reversed the expression levels of SLC7A11; However, SLC7A11 overexpression did not affect the expression levels of HIF-1α. So, we speculated that HIF-1α was the upstream regulatory gene of SLC7A11. Based on the predicted binding sites from the JASPAR database, we selected only the most promising candidates for validation. ChIP qPCR confirmed the interaction between HIF-1α and SLC7A11, further validating our hypothesis. Thus, we concluded that treatment with 2-ME2 alleviated the ferroptosis through the HIF-1α/SLC7A11 pathway. Due to the lack of effective treatment options for CIH-related lung injury, this discovery holds potential for clinical translation.

The study has some limitations. Firstly, the relatively small sample size used in the in vivo experiments may limit the generalizability and statistical robustness of the findings. Secondly, the in vitro experiments were confined to a single cell line, which may not fully capture the complexity and variability of the biological processes involved in the studied condition. To enhance the validity and applicability of the results, future research should consider expanding the sample size and including a more diverse range of cell models and experimental conditions.

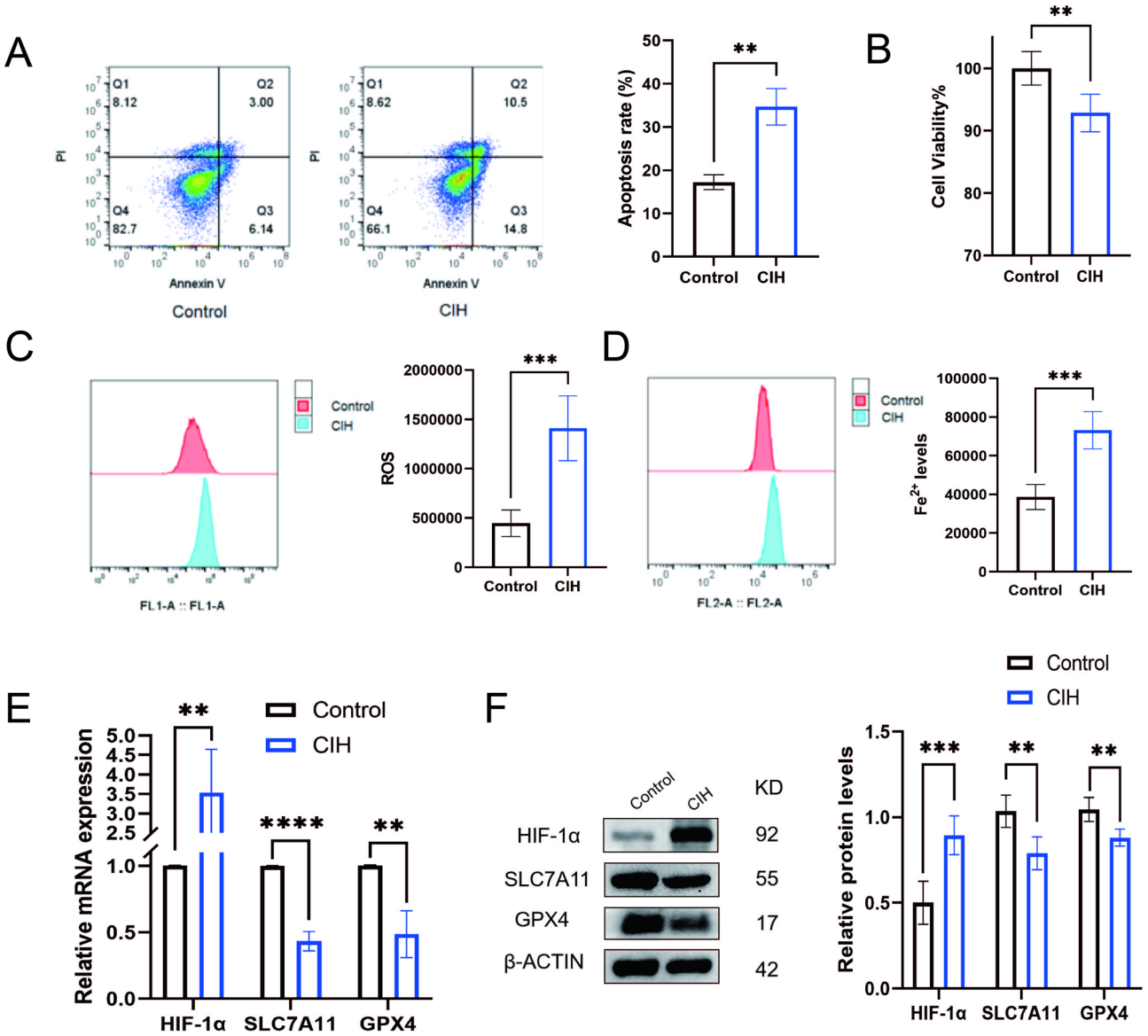

Fig. 3. CIH induced BEAS-2B injury and ferroptosis-related gene expression changes ($n = 5$); (**A**) CIH induced increased apoptosis rate compared with the control; (**B**), CIH induced decreased cell viability of BEAS-2B cells; (**C**), CIH induced increased ROS level compared with the control; (**D**), CIH induced increased Fe^{2+} levels in BEAS-2B cells compared with the control; (**E**), CIH upregulated HIF-1α mRNA while downregulating SLC7A11 and GPX4 mRNA compared with the control; (**F**), CIH upregulated HIF-1α protein and downregulated SLC7A11 and GPX4 protein levels compared with the control. Data are shown as the mean ± SD. ** $p < 0.01$; *** $p < 0.001$; **** $p < 0.0001$.

Conclusions

In conclusion, CIH-related lung injury and ferroptosis occurred both in vitro and in vivo. The HIF-1α inhibitor, 2-ME2, effectively reverses CIH-induced lung injury through the HIF-1α/SLC7A11 signaling pathway. Figure 6 displays a diagram summary. This study delved into the role and mechanism of ferroptosis in CIH-related lung injury and provided new ideas for potential targets of intervention treatment.

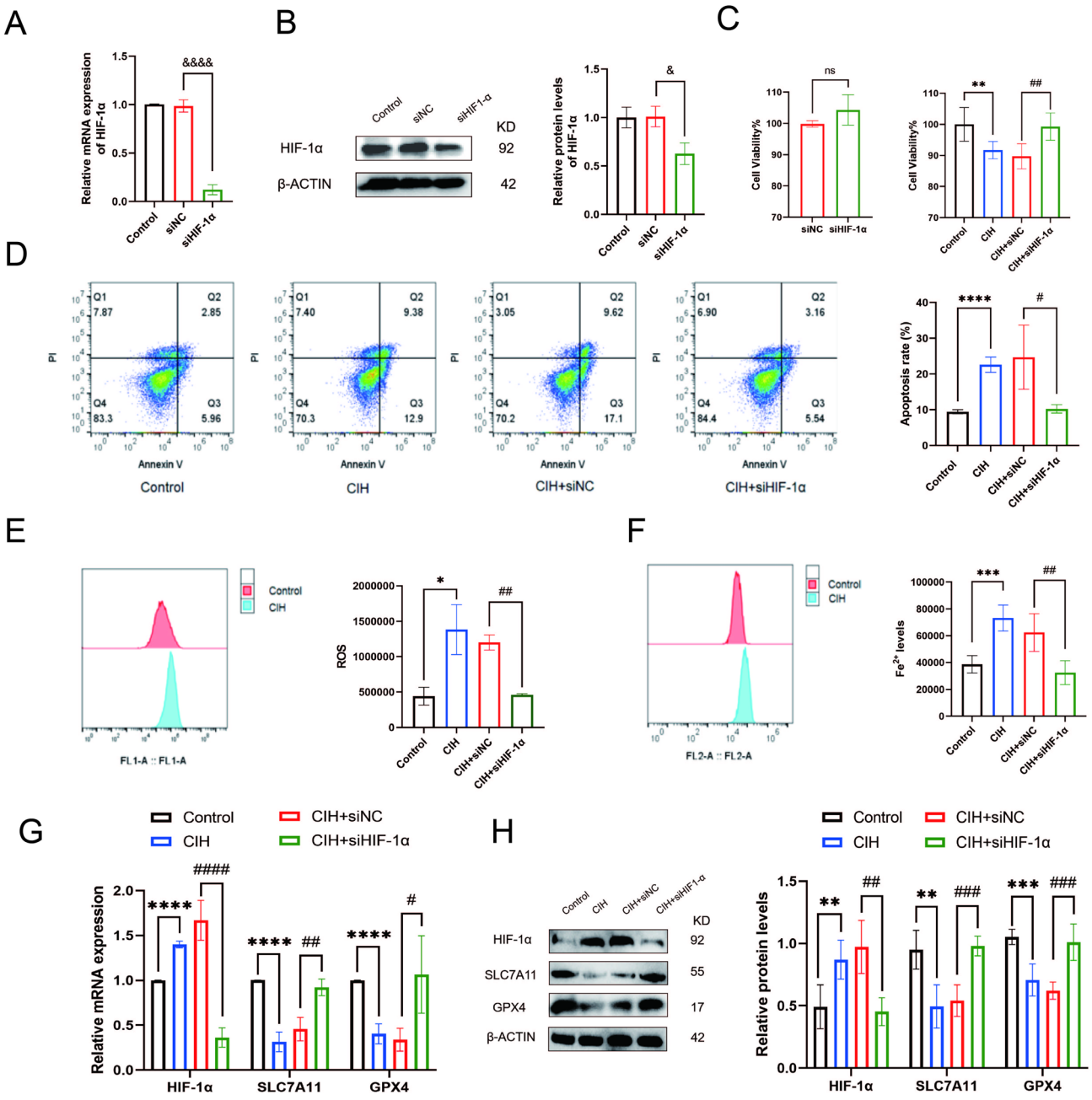

Fig. 4. CIH-induced ferroptosis is reversed after HIF-1α knockdown in the BEAS-2B cells ($n = 5$); (**A**) The transfection efficiency of HIF-1α siRNA was verified through qRT-PCR; (**B**), The transfection efficiency of HIF-1α siRNA was verified through Western Blot; (**C**), The cell viability of siNC and siHIF-1α shows no significant difference. HIF-1α knockdown reversed the decreased cell viability of BEAS-2B cells; (**D**), HIF-1α knockdown reversed the levels of apoptosis rate caused by CIH; (**E**), HIF-1α knockdown reversed the levels of ROS caused by CIH; (**F**), HIF-1α knockdown reversed the levels of Fe^{2+} caused by CIH; (**G**), HIF-1α knockdown reversed the mRNA levels of SLC7A11 and GPX4; (**H**), HIF-1α knockdown reversed the protein levels of SLC7A11 and GPX4. Data are shown as the mean ± SD. siHIF-1α compared with siNC: &$p < 0.05$; &&&&$p < 0.0001$. CIH compared with control: * $p < 0.05$; ** $p < 0.01$; *** $p < 0.001$; **** $p < 0.0001$; CIH + siHIF-1α compared with CIH + siNC: # $p < 0.05$; ## $p < 0.01$; ### $p < 0.001$; #### $p < 0.0001$.

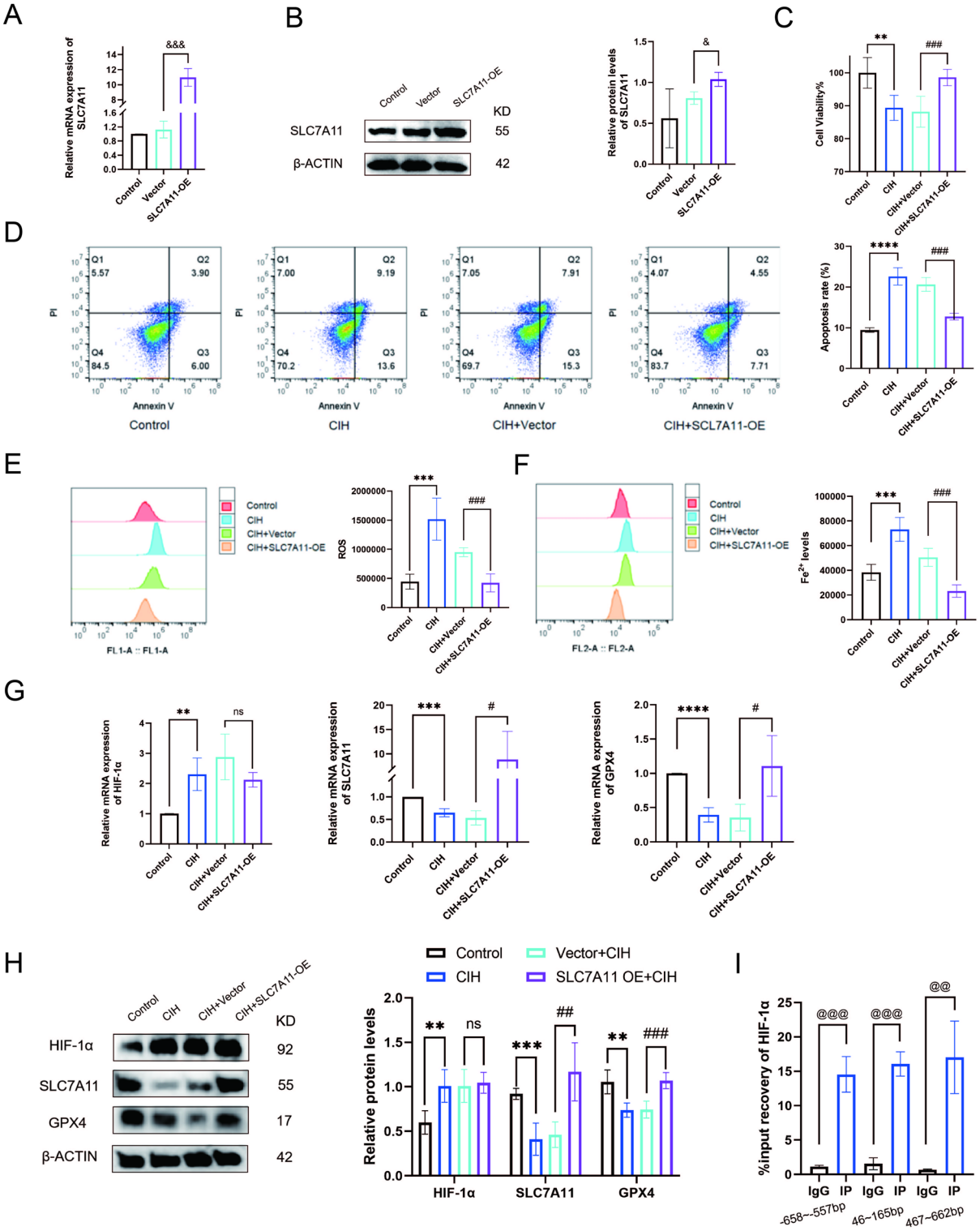
A
Relative mRNA expression of SLC7A11
&&&
Control
Vector
SLC7A11-OE
B
Control
Vector
SLC7A11-OE
KD
SLC7A11
55
β-ACTIN
42
Relative protein levels of SLC7A11
&
C
Cell Viability%
**
###
Control
CIH
CIH+Vector
CIH+SLC7A11-OE
D
Q1 5.57
Q2 3.90
Q4 84.5
Q3 6.00
Q1 7.00
Q2 9.19
Q4 70.2
Q3 13.6
Q1 7.05
Q2 7.91
Q4 69.7
Q3 15.3
Q1 4.07
Q2 4.55
Q4 83.7
Q3 7.71
PI
Annexin V
Control
CIH
CIH+Vector
CIH+SCL7A11-OE
Apoptosis rate (%)
****
###
E
Control
CIH
CIH+Vector
CIH+SLC7A11-OE
FL1-A :: FL1-A
ROS
***
###
F
FL2-A :: FL2-A
Fe2+ levels
G
Relative mRNA expression of HIF-1α
**
ns
Relative mRNA expression of SLC7A11
***
#
Relative mRNA expression of GPX4
****
#
H
Control
CIH
CIH+Vector
CIH+SLC7A11-OE
KD
HIF-1α
92
SLC7A11
55
GPX4
17
β-ACTIN
42
Control
Vector+CIH
CIH
SLC7A11 OE+CIH
Relative protein levels
HIF-1α
SLC7A11
GPX4
I
%input recovery of HIF-1α
@@@
@@@
@@
IgG
IP
-658~-557bp
46~165bp
467~662bp

◀**Fig. 5**. CIH-induced ferroptosis is reversed by the overexpression of SLC7A11 in the BEAS-2B cells ($n = 5$). (**A**) The transfection efficiency of SLC7A11 was verified through qRT-PCR; (**B**), The transfection efficiency of SLC7A11 was confirmed through Western Blot; (**C**), SLC7A11 overexpression reversed the viability of BEAS-2B cells; (**D**), SLC7A11 overexpression reversed the levels of apoptosis rate; (**E**), SLC7A11 overexpression reversed the levels of ROS; (**F**), SLC7A11 overexpression reversed the levels of Fe^{2+}; (**G**), SLC7A11 overexpression reversed the mRNA levels of GPX4, but did not affect the mRNA levels of HIF-1α; (**H**), SLC7A11 overexpression reversed the protein levels of GPX4, but did not affect the protein levels of HIF-1α. (**I**), A binding site exists between the HIF-1α and the promoter region of SLC7A11. ChIP-qPCR results showed that HIF-1α was significantly enriched in the SLC7A11 promoter region at -658–557 bp, 46–165 bp, and 467–662 bp, respectively. SLC7A11-OE compared with Vector: &$p < 0.05$; &&&$p < 0.001$; CIH compared with control: **$p < 0.01$; *** $p < 0.001$; ****$p < 0.0001$; CIH + SLC7A11-OE compared with CIH + Vector: #$p < 0.05$; ##$p < 0.01$; ###$p < 0.001$; ns $p > 0.05$; IgG IP compared with HIF-1α IP: @@$p < 0.01$; @@@$p < 0.001$.

Matrix ID	Name	Score	Relative score	Sequence ID	Start	End	Strand	Predicted sequence
MA0259.1	MA0259.1.ARNT::HIF1A	9.542456	0.950580150990242	SLC7A11	2481	2488	+	GGGCGTGC
MA0259.1	MA0259.1.ARNT::HIF1A	7.0066285	0.8749302281145968	SLC7A11	1638	1645	-	ATGCGTGT
MA1106.1	MA1106.1.HIF1A	5.7179556	0.8267549024074725	SLC7A11	2481	2490	+	GGGCGTGCTC
MA0259.1	MA0259.1.ARNT::HIF1A	4.79955	0.8090876826584762	SLC7A11	1442	1449	+	GTATGTGA
MA0259.1	MA0259.1.ARNT::HIF1A	4.579703	0.8025291032088911	SLC7A11	2053	2060	+	GGAGGTGG
MA0259.1	MA0259.1.ARNT::HIF1A	4.5247393	0.8008894050019273	SLC7A11	1795	1802	+	GTGTGTGC

Table 4. Prediction of HIF-1α binding sites in SLC7A11.

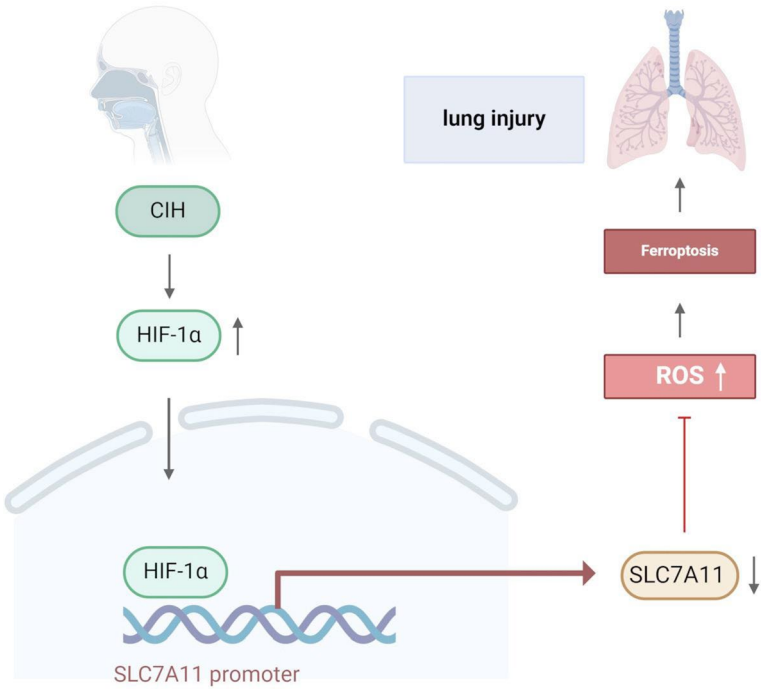

Fig. 6. A diagram depicting the HIF-1α/SLC7A11 pathway in CIH-induced lung injury. CIH activates HIF-1α, which then binds to the SLC7A11 promoter, resulting in the downregulation of SLC7A11. This downregulation leads to ROS accumulation and ferroptosis, ultimately causing lung injury.

Data availability

The datasets generated during and analyzed during the current study are available from the corresponding author on reasonable request.

Received: 13 October 2024; Accepted: 15 May 2025
Published online: 21 May 2025

References

1. Badran, M., Bender, S. B. & Gozal, D. *Cardiovascular disease in obstructive sleep apnea: putative contributions of mineralocorticoid receptors*. *Int. J. Mol. Sci.*, **24**(3). (2023).
2. Meliante, P. G. et al. *Molecular pathology, oxidative stress, and biomarkers in obstructive sleep apnea*. *Int. J. Mol. Sci.*, **24**(6). (2023).
3. Locke, B. W., Lee, J. J. & Sundar, K. M. *OSA and chronic respiratory disease: mechanisms and epidemiology*. *Int. J. Environ. Res. Public. Health*, **19**(9). (2022).
4. Ou, Y. H., Tan, A. & Lee, C. H. Management of hypertension in obstructive sleep apnea. *Am. J. Prev. Cardiol.* **13**, 100475 (2023).
5. Bassetti, C. & Aldrich, M. S. Sleep apnea in acute cerebrovascular diseases: final report on 128 patients. *Sleep* **22** (2), 217–223 (1999).
6. Chen, L. D. et al. The role of ferroptosis in chronic intermittent hypoxia-induced liver injury in rats. *Sleep. Breath.* **24** (4), 1767–1773 (2020).
7. Tang, M. et al. Risk for cardiovascular disease and One-Year mortality in patients with chronic obstructive pulmonary disease and obstructive sleep apnea syndrome overlap syndrome. *Front. Pharmacol.* **12**, 767982 (2021).
8. Zhou, W. et al. Metabolic syndrome prevalence in patients with obstructive sleep apnea syndrome and chronic obstructive pulmonary disease: relationship with systemic inflammation. *Clin. Respir J.* **14** (12), 1159–1165 (2020).
9. Wang, J. et al. Endothelial function and T-lymphocyte subsets in patients with overlap syndrome of chronic obstructive pulmonary disease and obstructive sleep apnea. *Chin. Med. J. (Engl)*. **132** (14), 1654–1659 (2019).
10. Fitzgibbons, C. M. et al. Physical activity in overlap syndrome of COPD and obstructive sleep apnea: relationship with markers of systemic inflammation. *J. Clin. Sleep. Med.* **15** (7), 973–978 (2019).
11. Troy, L. K. & Corte, T. J. Sleep disordered breathing in interstitial lung disease: A review. *World J. Clin. Cases*. **2** (12), 828–834 (2014).
12. Wang, Y. et al. Obstructive sleep apnea exacerbates airway inflammation in patients with chronic obstructive pulmonary disease. *Sleep. Med.* **16** (9), 1123–1130 (2015).
13. Alkhalil, M., Schulman, E. & Getsy, J. Obstructive sleep apnea syndrome and asthma: what are the links? *J. Clin. Sleep. Med.* **5** (1), 71–78 (2009).
14. Yang, Q. C. et al. Systematic and endothelial inflammation and endothelial progenitor cell levels in emphysematous rats exposed to intermittent hypoxia. *Respir Care*. **60** (2), 279–289 (2015).
15. Haslip, M. et al. Endothelial uncoupling protein 2 regulates mitophagy and pulmonary hypertension during intermittent hypoxia. *Arterioscler. Thromb. Vasc Biol.* **35** (5), 1166–1178 (2015).
16. Papachatzakis, I. et al. Comorbidities in coexisting chronic obstructive pulmonary disease and obstructive sleep apnea - overlap syndrome. *Eur. Rev. Med. Pharmacol. Sci.* **22** (13), 4325–4331 (2018).
17. Economou, N. T. et al. Sleepiness, fatigue, anxiety and depression in chronic obstructive pulmonary disease and obstructive sleep Apnea - Overlap - Syndrome, before and after continuous positive airways pressure therapy. *PLoS One*. **13** (6), e0197342 (2018).
18. Adler, D. et al. Clinical presentation and comorbidities of obstructive sleep apnea-COPD overlap syndrome. *PLoS One*. **15** (7), e0235331 (2020).
19. Dixon, S. J. et al. Ferroptosis: an iron-dependent form of nonapoptotic cell death. *Cell* **149** (5), 1060–1072 (2012).
20. Chen, J. et al. The role of ferroptosis in chronic intermittent hypoxia-induced lung injury. *BMC Pulm Med.* **22** (1), 488 (2022).
21. Pezzuto, A. & Carico, E. Role of HIF-1 in Cancer progression: novel insights. A review. *Curr. Mol. Med.* **18** (6), 343–351 (2018).
22. Semenza, G. L. Targeting HIF-1 for cancer therapy. *Nat. Rev. Cancer*. **3** (10), 721–732 (2003).
23. Prabhakar, N. R., Peng, Y. J. & Nanduri, J. Hypoxia-inducible factors and obstructive sleep apnea. *J. Clin. Invest.* **130** (10), 5042–5051 (2020).
24. Gao, X. et al. The mechanisms of ferroptosis under hypoxia. *Cell. Mol. Neurobiol.* **43** (7), 3329–3341 (2023).
25. Lei, G. et al. Ferroptosis, radiotherapy, and combination therapeutic strategies. *Protein Cell.* **12** (11), 836–857 (2021).
26. Zou, Y. et al. A GPX4-dependent cancer cell state underlies the clear-cell morphology and confers sensitivity to ferroptosis. *Nat. Commun.* **10** (1), 1617 (2019).
27. Fan, X. X. et al. Honokiol improves depression-like behaviors in rats by HIF-1α- VEGF signaling pathway activation. *Front. Pharmacol.* **13**, 968124 (2022).
28. Liao, W. I. et al. 2-Methoxyestradiol protects against lung ischemia/reperfusion injury by upregulating Annexin A1 protein expression. *Front. Immunol.* **12**, 596376 (2021).
29. Elzayat, M. A. et al. Ameliorative effect of 2-methoxyestradiol on radiation-induced lung injury. *Life Sci.* **255**, 117743 (2020).
30. Yaman, O. M. et al. *Protective effect of thymosin B4 against abdominal aortic Ischemia-Reperfusion-Induced acute lung injury in rats*. *Med. (Kaunas)*, **55**(5). (2019).
31. Miao, S. et al. The potential effects of Aliskiren on atrial remodeling induced by chronic intermittent hypoxia in rats. *Drug Des. Devel Ther.* **14**, 3755–3764 (2020).
32. Xuan, W. et al. Gut microbiota-derived acetic acids promoted sepsis-induced acute respiratory distress syndrome by delaying neutrophil apoptosis through FABP4. *Cell. Mol. Life Sci.* **81** (1), 438 (2024).
33. Li, Y. et al. Pterostilbene pre-treatment reduces LPS-induced acute lung injury through activating NR4A1. *Pharm. Biol.* **60** (1), 394–403 (2022).
34. Jiang, X., Stockwell, B. R. & Conrad, M. Ferroptosis: mechanisms, biology and role in disease. *Nat. Rev. Mol. Cell. Biol.* **22** (4), 266–282 (2021).
35. Rochette, L. et al. *Lipid peroxidation and Iron metabolism: two corner stones in the homeostasis control of ferroptosis*. *Int. J. Mol. Sci.*, **24**(1). (2022).
36. , D. N.J. et al. Oxytosis/Ferroptosis in neurodegeneration: the underlying role of master regulator glutathione peroxidase 4 (GPX4). *Mol. Neurobiol.* **61** (3), 1507–1526 (2024).
37. Bastian, P. et al. *Regulation of Mitochondrial Dynamics in Parkinson's Disease-Is 2-Methoxyestradiol a Missing Piece?*. *Antioxid. (Basel)*, **10**(2). (2021).
38. Gabryelska, A. et al. Patients with obstructive sleep apnea present with chronic upregulation of serum HIF-1α protein. *J. Clin. Sleep. Med.* **16** (10), 1761–1768 (2020).
39. Gabryelska, A. et al. Serum hypoxia-inducible factor-1α protein level as a diagnostic marker of obstructive sleep apnea. *Pol. Arch. Intern. Med.* **130** (2), 158–160 (2020).
40. Gabryelska, A. et al. Influence of one-night CPAP therapy on the changes of HIF-1α protein in OSA patients: A pilot study. *J. Sleep. Res.* **29** (4), e12995 (2020).
41. Yuan, S. et al. Sorafenib attenuates liver fibrosis by triggering hepatic stellate cell ferroptosis via HIF-1α/SLC7A11 pathway. *Cell. Prolif.* **55** (1), e13158 (2022).
42. Fan, Z. et al. Hypoxia blocks ferroptosis of hepatocellular carcinoma via suppression of METTL14 triggered YTHDF2-dependent Silencing of SLC7A11. *J. Cell. Mol. Med.* **25** (21), 10197–10212 (2021).
43. Chen, L., Luo, S. & Tan, H. Penehyclidine hydrochloride improves Rhabdomyolysis-Mediated acute kidney injury by inhibiting ferroptosis through the HIF-1α/MT1G Axis. *Nephron* **148** (5), 333–344 (2024).

Author contributions

All authors contributed to the study's conception and design.NFL was in charge of designing and supervising

the study. JC wrote the first manuscripts. JC performed the experiments and conceived the study. NFL, JC, HSX, WQC, TL, SYH, YQL, and JFH performed material preparation, data collection, and analysis. All authors reviewed and approved the final manuscript. All statements contained in it purporting to be factual are true and correct. All authors agreed to be accountable for all aspects of the work.

Funding
This study was funded by the National Natural Science Foundation of China (No. 82170101), the National Natural Science Foundation of China (No. 82470082), Joint Funds for the Innovation of Science and Technology, Fujian Province (No. 2023Y9024).

Declarations

Competing interests
The authors declare no competing interests.

Ethics approval and consent to participate
The Ethics Committee of the Fujian Medical University Laboratory Animal Center approved this study (approve number: IACUCFJMU2022-0031). We verified that the study was reported following ARRIVE guidelines, and all methods were performed in conformity with relevant guidelines and regulations.

Additional information
Supplementary Information The online version contains supplementary material available at https://doi.org/10.1038/s41598-025-02675-8.

Correspondence and requests for materials should be addressed to N.L.

Reprints and permissions information is available at www.nature.com/reprints.

Publisher's note Springer Nature remains neutral with regard to jurisdictional claims in published maps and institutional affiliations.